

# Mitochondrial ATP Synthasome

THREE-DIMENSIONAL STRUCTURE BY ELECTRON MICROSCOPY OF THE ATP SYNTHASE IN COMPLEX FORMATION WITH CARRIERS FOR P<sub>i</sub> AND ADP/ATP\*

Received for publication, February 6, 2004, and in revised form, May 13, 2004  
Published, JBC Papers in Press, May 27, 2004, DOI 10.1074/jbc.M401353200

Chen Chen<sup>‡</sup>, Young Ko<sup>§</sup>, Michael Delannoy<sup>¶</sup>, Steven J. Ludtke<sup>||</sup>, Wah Chiu<sup>||</sup>,  
and Peter L. Pedersen<sup>‡\*\*</sup>

From the <sup>‡</sup>Department of Biological Chemistry, the <sup>§</sup>Russell H. Morgan Department of Radiology and Radiological Sciences, and the <sup>¶</sup>Department of Cell Biology and Anatomy, Johns Hopkins University, School of Medicine, Baltimore, Maryland 21205-2185 and the <sup>||</sup>National Center for Macromolecular Imaging, Vern and Marrs McLean Department of Biochemistry and Molecular Biology, Baylor College of Medicine, Houston, Texas 77030

The terminal steps involved in making ATP in mitochondria require an ATP synthase (F<sub>0</sub>F<sub>1</sub>) comprised of two motors, a phosphate carrier (PIC), and an adenine nucleotide carrier (ANC). Under mild conditions, these entities sub-fractionate as an ATP synthase/PIC/ANC complex or “ATP synthasome” (Ko, Y.H., Delannoy, M, Hüllihen, J., Chiu, W., and Pedersen, P.L. (2003) *J. Biol. Chem.* 278, 12305–12309). As a first step toward obtaining three-dimensional information about this large complex or “metabolon” and the locations of PIC and ANC therein, we dispersed ATP synthasomes into single complexes and visualized negatively stained images by electron microscopy (EM) that showed clearly the classical headpiece, central stalk, and basepiece. Parallel immuno-EM studies revealed the presence of PIC and ANC located non-centrally in the basepiece, and other studies implicated an ATP synthase/PIC/ANC stoichiometry near 1:1:1. Single ATP synthasome images (7506) were boxed, and, using EMAN software, a three-dimensional model was obtained at a resolution of 23 Å. Significantly, the basepiece is oblong and contains two domains, the larger of which connects to the central stalk, whereas the smaller appears as an extension. Docking studies with known structures together with the immuno-EM studies suggest that PIC or ANC may be located in the smaller domain, whereas the other transporter resides nearby in the larger domain. Collectively, these findings support a mechanism in which the entry of the substrates ADP and P<sub>i</sub> into mitochondria, the synthesis of ATP on F<sub>1</sub>, and the release and exit of ATP are very localized and highly coordinated events.

Animal mitochondria have two major roles, one of which is to participate in cell life by making ATP by a process known as oxidative phosphorylation (1), and the other role is to participate in cell death, either by apoptosis or necrosis (2, 3). During oxidative phosphorylation the ATP synthase works in the direction of ATP synthesis, whereas during necrotic cell death the enzyme works in the direction of ATP hydrolysis (3, 4). When working in the direction of ATP synthesis in intact

mitochondria, the enzyme has an absolute dependence on the P<sub>i</sub> and ADP/ATP carriers, PIC<sup>1</sup> and ANC, respectively (5). These carriers supply the ATP synthase with its essential substrates to make ATP, and ANC also transports ATP out of the mitochondria to energize numerous cellular processes (Fig. 1A).

The ATP synthase has attracted considerable attention in recent years, not only because of its involvement in cell life and necrotic cell death, but also because of the unique and remarkable mechanism by which it makes ATP (6–10). Although a consensus has not been reached on all points, it seems clear that the synthase consists of two nanomotors (11), one called F<sub>1</sub>, which is driven by ATP hydrolysis, and the other contained within F<sub>0</sub>, which is driven by a proton gradient. During oxidative phosphorylation in mitochondria (Fig. 1A), the electron transport chain generates a proton gradient that is purported to drive the rotation of a central rotor located in the nanomotor contained within F<sub>0</sub>. This rotation, in turn, is believed to drive in reverse the rotation of a central rotor within the F<sub>1</sub> nanomotor, inducing via a conformational change the sequential release of bound ATP at three identical catalytic sites followed by the sequential synthesis of newly formed ATP from P<sub>i</sub> and ADP at these sites. In close synchrony with these events, and obligatory for them, is the entry of P<sub>i</sub> and ADP on the transporters PIC and ANC, respectively, and the exit on ANC of the ATP released from the synthase.

On the basis of the above outline, it is not surprising that in mitochondria the ATP synthase and its associated substrate suppliers, PIC and ANC, can form a complex, one which we have recently isolated in intact form from liver mitochondria and named the “ATP synthasome” (12). This terminal complex of oxidative phosphorylation is very large, exhibiting a molecular mass of at least 0.7 million and is comprised of 17 subunit types and >30 total subunits. Specifically, the F<sub>1</sub> nanomotor contains five subunit types in the stoichiometric ratio α<sub>3</sub>β<sub>3</sub>γδε (13), whereas the nanomotor within F<sub>0</sub> contains four subunit types that include three found in bacteria in the apparent stoichiometric ratio ab<sub>2</sub>c<sub>10–14</sub> plus the subunit called the oligomycin sensitivity-conferring protein. The remaining eight subunit types include the six F<sub>0</sub> “supernumerary” subunits d, e, f, g, F<sub>6</sub>, and A6L together with PIC and ANC. Two regulatory proteins, an inhibitor called IF<sub>1</sub> (14) and an activator named

\* Supported by National Institutes of Health Grants CA 10951 (to P. L. P.) and P41RR02250 (to W. C.) for the National Center for Macromolecular Imaging. The costs of publication of this article were defrayed in part by the payment of page charges. This article must therefore be hereby marked “advertisement” in accordance with 18 U.S.C. Section 1734 solely to indicate this fact.

\*\* To whom correspondence should be addressed. Tel.: 410-955-3827; Fax: 410-614-1944; E-mail: ppederse@jhmi.edu.

<sup>1</sup> The abbreviations used are: PIC, phosphate carrier; ANC, adenine nucleotide carrier; ATP synthasome, ATP synthase/PIC/ANC complex; CHAPS, 3-[3-cholamidopropyl] dimethylammonio]-1-propane sulfonate; AMP-PCP, α,β-methylene-adenosine-5'-triphosphate; SH, sulfhydryl; Tricine, N-[2-hydroxy-1,1-bis(hydroxymethyl)ethyl]glycine.

factor B (15), are not readily detected in our isolated ATP synthasome preparation (12), as they are released upon purification.

To fully understand how the complete mitochondrial ATP synthasome works during oxidative phosphorylation necessitates the acquisition of a three-dimensional structure at atomic resolution. Although such structures have been obtained for the  $F_1$  moiety (16–18), no atomic resolution structure is available for the mitochondrial ATP synthasome. As a first step toward obtaining three-dimensional information, we screened previously over 80 different detergents to identify those that maintain these complexes dispersed and active, with retention of sensitivity to inhibition by oligomycin (12). Here, we report a three-dimensional image reconstruction of the complete 17-subunit-type mitochondrial ATP synthasome of rat liver at a 23-Å resolution obtained by dispersing the purified preparation into individual complexes in one of the promising detergents (CHAPS).

#### EXPERIMENTAL PROCEDURES

**Materials**—Rats (Harlan Sprague-Dawley<sup>CD</sup>, white males) were obtained from Charles River Breeding Laboratories. The detergents digitonin and Lubrol WX, used to subfractionate the mitochondria (12), were obtained from Calbiochem and Grand Island Biologicals, respectively, whereas the detergent CHAPS was obtained from Anatrache. The antibody to PIC (residues 302–312) was from our own stock, whereas the ANC antibody was obtained from Santa Cruz Biotechnology. Oligomycin and AMP-PCP were obtained from Sigma, Coomassie dye was from Pierce, and all materials for electron microscopy (EM) were from Ted Pella. All other materials were of the highest purity commercially available.

**ATP Synthasomes**—These were made exactly as described (12) starting with purified inner membrane vesicles of rat liver mitochondria and then extensively subfractionating and washing these vesicles to provide a population of highly enriched, cristae-like membranes containing the ATP synthase, PIC, and ANC, which sedimented as a single ATP synthase/PIC/ANC complex on a sucrose gradient. ATP synthasomes used for these studies exhibited an ATPase-specific activity in the range of 15–20  $\mu\text{mol ATP hydrolyzed} \times \text{min}^{-1} \times \text{mg}^{-1}$  and were inhibited 90% or more by oligomycin.

**ATPase Activity**—ATP synthasome or  $F_1$  preparations were assayed for ATPase activity with and without oligomycin (0.6  $\mu\text{g}/\text{mg}$  protein) by a previously described spectrophotometric procedure (19) that couples the ADP formed in the ATPase reaction to the pyruvate kinase and lactic dehydrogenase reactions and monitors the decrease in absorption at 340 nm as NADH is converted to  $\text{NAD}^+$ .

**Determination of Protein**—For preparation of the inner mitochondrial membrane, protein was determined by the biuret procedure (20). For ATP synthasomes, protein was determined by using either the method of Lowry *et al.* (21) or the Coomassie dye binding procedure (Pierce). In all cases, the standard used was bovine albumin. For determining the stoichiometry of the ATP synthase, PIC, and ANC within the ATP synthasome complex, the following four assays were used: (i) Coomassie dye binding (Pierce); (ii) Lowry (21); (iii) bicinchoninic (BCA) (22); and (iv) filter (23). Here, both bovine albumin and lysozyme were used as standard.

**Determination of Free SH Groups**—Free SH groups were determined for the ATP synthasome using Ellman's reagent (5,5'-dithiobis(2-nitrobenzoic acid)) (24). The final purified ATP synthasome membrane fraction was washed twice in KE buffer (100 mM potassium  $\text{P}_i$ , 1 mM EDTA, pH 7.9) and solubilized with 0.6% *n*-decyl- $\beta$ -D-thiomaltopyranoside in the same buffer to give a protein concentration of 2 mg/ml. The fraction was subjected then to sedimentation at 4 °C for 10 h in a sucrose gradient (0–25%) buffered with 100 mM potassium  $\text{P}_i$ , 10 mM EDTA, 4 mM ATP, 5% ethylene glycol, 25% sucrose, and 0.3% *n*-decyl- $\beta$ -D-thiomaltopyranoside, pH 7.4. Sedimentation was carried out in a SW28 rotor in a Beckman Optima LE 80 K ultracentrifuge. Each fraction from the resulting sucrose gradient was analyzed for its protein concentration, ATPase activity, and oligomycin sensitivity. Then, the peak fraction was denatured in 1% SDS for 15 min at 25 °C, after which the total number of SH groups was determined with 5,5'-dithiobis(2-nitrobenzoic acid) by measuring the absorbance at 412 nm. Varying concentrations of cysteine served for generating a standard curve. The protein concentration was averaged, based on the four protein assays listed above, and used for calculation of the total number of SH groups per mole of

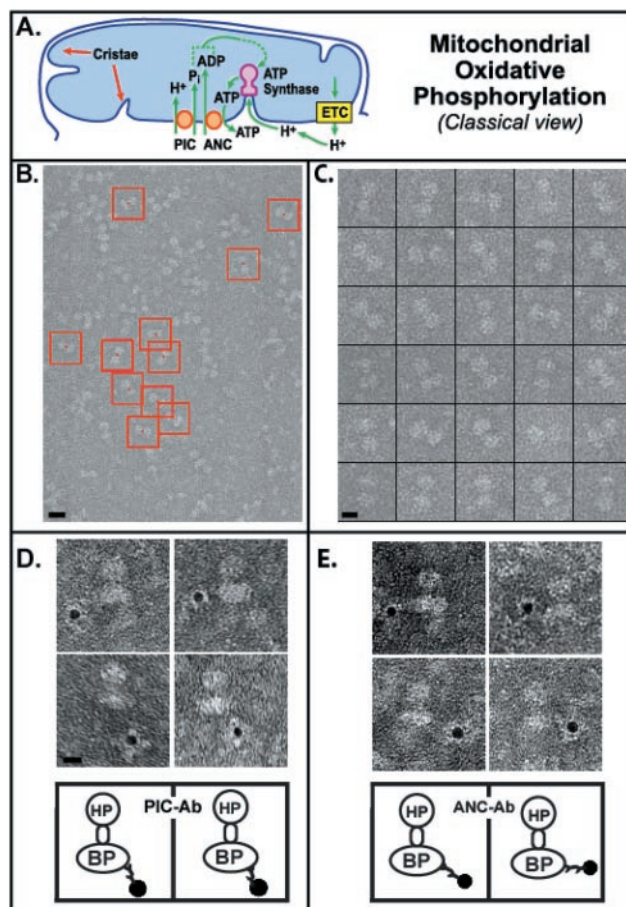
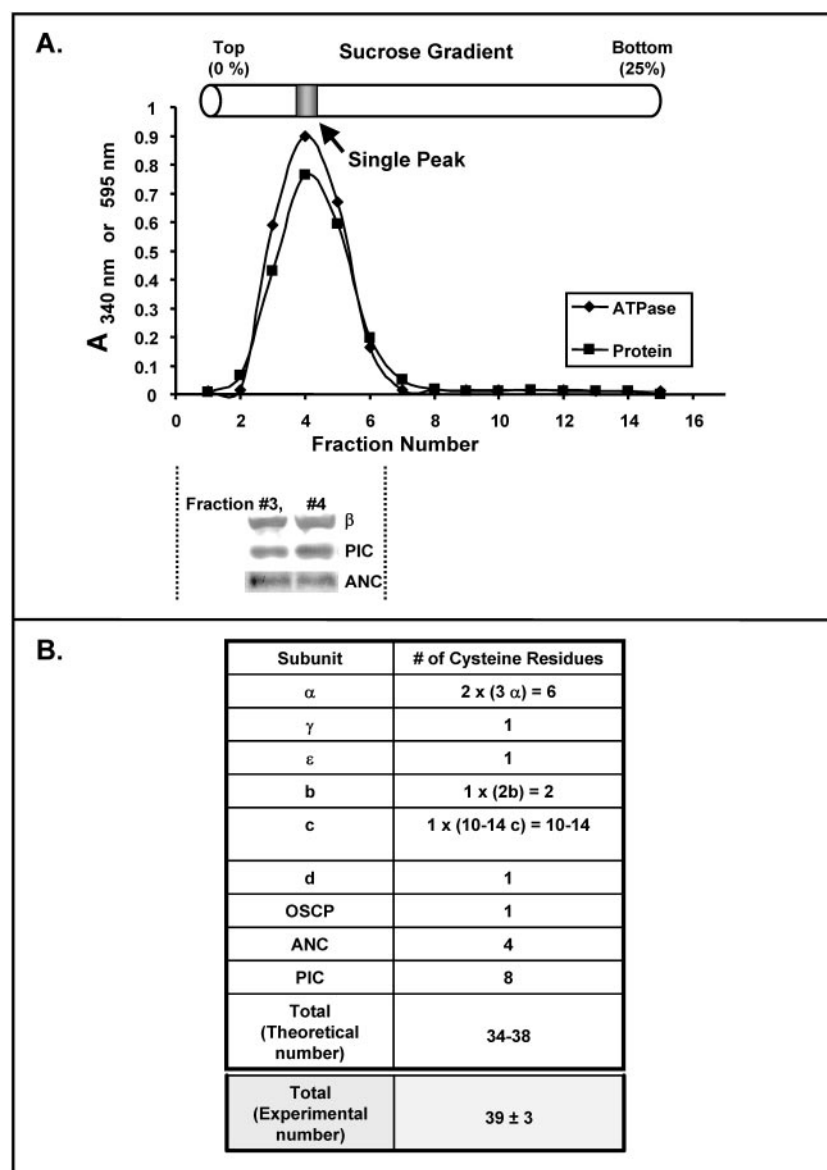


FIG. 1. A, simplified “classical” view of mitochondrial structure and function. The major function of mitochondria is to produce ATP by a process called oxidative phosphorylation. This process involves an electron transport chain (ETC) that generates an electrochemical gradient of protons that drives the synthesis of ATP from ADP and  $\text{P}_i$  via the ATP synthase ( $F_0F_1$ ). The proton gradient also drives the uptake of  $\text{P}_i$  on a phosphate carrier, PIC, whereas ADP enters the mitochondria on the adenine nucleotide carrier, ANC. When ATP is made on the ATP synthase, it is transported out of the mitochondria on the ANC in exchange for the entry of an ADP molecule. Classically, the inner membrane is viewed as folding inward to form “cristae” that contain the ATP synthase molecules. Also classically, the ATP synthase, PIC, and ANC are viewed as existing as separate entities in the membrane, although recently we have provided evidence that they co-localize as an ATP synthase/PIC/ANC complex that we have named the ATP synthasome (12). B, a dispersed preparation of ATP synthasomes prepared from rat liver mitochondria as described previously (12). After preparation, ATP synthasomes were dispersed with the detergent CHAPS, adsorbed onto parlodion-carbon-coated copper grids, negatively stained with 1% uranyl acetate, and visualized and photographed using the Philips CM120 electron microscope operated in the low dose mode at an under-focus of 0.5–2.0  $\mu\text{m}$ , a magnification of 37,000, and an accelerating voltage of 80 kV. The scale bar equals 200 Å. C, gallery of boxed ATP synthasomes. Negatives in B and other similar negatives were scanned at 14- $\mu\text{m}$  increments corresponding to 3.78 Å/pixel. Images of individual ATP synthasomes were then boxed at 100  $\times$  100 pixels. Each ATP synthasome shows a characteristic “dumbbell-like” shape or tripartite appearance with a near spherical part (head), a nonspherical part (basepiece), and a connecting segment (stalk). Each negative was evaluated by an inspection of its two-dimensional power spectrum calculated by the EMAN program (25). Negatives exhibiting a spherical shaped power spectrum were used in subsequent steps, whereas those with ellipsoidal or other shapes were considered to be defective because of astigmatism or drift and excluded. A total of 7506 single images regarded as “good” were obtained. The scale bar equals 100 Å. D and E, verification that PIC and ANC are present in individual ATP synthasomes. Using antibodies specific for PIC (D) and ANC (E) and a gold-conjugated secondary antibody, immuno-EM studies were carried out on dispersed preparations of ATP synthasomes as described under “Experimental Procedures.” The bottom panels in D and E provide a pictorial interpretation of how the secondary gold-labeled antibody projects from the basepiece of the ATP synthasomes shown in the center panels. HP, headpiece; BP, basepiece. The scale bar in D equals 100 Å.

FIG. 2. A, demonstration that the proteins comprising the ATP synthasome, *i.e.* the ATP synthase, PIC, and ANC, sediment as a single species following detergent solubilization. The purified ATP synthasome fraction was solubilized in 0.5% *n*-decyl- $\beta$ -D-thiomaltopyranoside and subjected to sedimentation for 10 h at 25,000 rpm in a 0–25% sucrose gradient as described previously (12). Fractions were then collected, assayed for protein and ATPase activity as described under “Experimental Procedures,” and subjected to Western analysis (12). B, determination of free SH groups. These were determined for the ATP synthasome using Ellman’s reagent, (5,5’-dithiobis(2-nitrobenzoic acid)) (24) exactly as indicated under “Experimental Procedures.” OSCP, oligomycin sensitivity-conferring protein.



protein. The molecular mass of the ATP synthasome was estimated as 706,210 Da based on known subunit sequences and stoichiometries.

**Electron Microscopy**—A 1-ml solution containing 1 mM ADP, 1 mM AMP-PCP, 2 mM  $MgCl_2$ , 5 mM EDTA, 5% ethylene glycol, 1% CHAPS, and 10  $\mu$ g/ml ATP synthasomes, pH 7.5 was centrifuged at 14,000 rpm in a desktop centrifuge for 5 min. The resultant supernatant was then adsorbed onto glow-discharged carbon/parlodion-coated copper grids and stained with 1% uranyl acetate containing 0.02% tylose. After removing the excess negative stain by blotting and then air drying, ATP synthasome samples on the grid were visualized under a Philips CM120 electron microscope in a low dose mode at an accelerating voltage of 80 kV, a magnification of 37,000 $\times$ , and under-focus settings ranging from 0.5 to 2  $\mu$ m.

**Two-dimensional Analysis and Three-dimensional Reconstruction of the ATP Synthasome**—The negatives were scanned at 14- $\mu$ m increments corresponding to 3.78  $\text{\AA}$ /pixel using the Zeiss SCAI scanner. The program EMAN (25) was used for image processing. A power spectrum was calculated to assess image quality. Negatives exhibiting astigmatism were excluded, whereas ATP synthasome particles in acceptable negatives were “boxed” at  $100 \times 100$  pixels, normalized, and combined to give one raw image file. A total of 7506 individual ATP synthasome images were obtained.

For two-dimensional analysis, the 7506 single ATP synthasome images were contrast transfer function phase-corrected, band pass-filtered, and subjected to multivariate statistical analysis. First, these raw images were iteratively aligned to each other and subjected to singular value decomposition to produce a set of orthogonal basis vec-

tors (26). Then the aligned raw images were classified into 25 groups based on classification of images projected into a basis subspace (25).

For three-dimensional reconstruction, the 7506 ATP synthasome images were reconstructed using the standard refinement technique in EMAN (25). Because virtually all of the selected particles were side views, meaning they shared a single common line, common lines could not be used to assign particle orientations. Instead, the unaligned images were classified by the k-means method based on rotational and translational invariance to produce 56 class averages. Then, apparent side view class averages were assigned random azimuthal orientations to produce a starting model. This model was then iteratively refined using the EMAN program’s standard iterative projection matching-based approach until a self-consistent result was obtained. Although this procedure appears rather arbitrary, the EMAN refinement loop has an extremely broad radius of convergence, and it has been demonstrated many times that very little is required in most cases to obtain an unambiguous final result. For example, a 6- $\text{\AA}$  resolution GroEL structure has been successfully refined from a featureless ellipsoid starting model.<sup>2</sup> Resolution of the final ATP synthasome structure was measured using the standard Fourier shell coefficient method (26) applied to models calculated using only the even- and odd-numbered particles, respectively, at a 0.5 threshold value.

**Immuno-electron Microscopy**—Purified ATP synthasomes and the antibody to either PIC or ANC were mixed and solubilized in 200  $\mu$ l of

<sup>2</sup> S. J. Ludkte, unpublished observation.

TA buffer (50 mM Tricine, 1 mM ATP, 25 mM EDTA, 0.5 mM dithiothreitol, and 0.5% ethylene glycol, pH 7.9) to give a final concentration of 500  $\mu\text{g/ml}$  ATP synthasomes and 100  $\mu\text{g/ml}$  antibody. After incubating and constantly inverting the mixture for 1 h, TA buffer was added to reduce the final concentration of CHAPS to 0.1%. After standing on ice for 1 h, centrifugation was carried out at 48,000 rpm for 30 min in a 70.1-Ti rotor in a Beckman Optima LE 80K ultracentrifuge. The supernatant was discarded, and the pellet containing the ATP synthasome-antibody complex was suspended again in TA buffer (20  $\mu\text{l}$ ). An aliquot was solubilized in TA buffer containing 0.5% CHAPS to give a final concentration of  $\sim 10$   $\mu\text{g/ml}$ . The sample was then adsorbed onto glow-discharged parlodion/carbon-coated copper grids. After cross-linking briefly with 0.2% glutaraldehyde and blocking with 1% normal serum, the grid was probed with a gold-conjugated anti-rabbit IgG and subjected to negative staining with 1% uranyl acetate containing 0.02% tylose. After air drying, the image was observed under the Philips CM120 electron microscope with an accelerating voltage of 80 kV and a nominal magnification of 155,000. The resultant negatives were scanned with a Zeiss SCAI scanner with a 56- $\mu\text{m}$  step size.

## RESULTS

**Stabilization, Dispersion, and Visualization of ATP Synthasomes**—The final purified preparation of ATP synthasomes was obtained in insoluble form as described previously (12). Prior to examining this fraction by EM, it was solubilized in a mixture containing the detergent CHAPS,  $\text{MgCl}_2$ , EDTA, ADP, and AMP-PCP, a nonhydrolyzable ATP analog. This strategy was used to maintain each ATP synthasome in a single stable conformation with MgADP and MgAMP-PCP while obtaining a high degree of dispersion with CHAPS. Following centrifugation to remove any insoluble protein (almost negligible), the preparation was adsorbed onto glow discharged, carbon/parlodion-coated copper grids, negatively stained with uranyl acetate, and subjected to EM. This approach resulted in the visualization of numerous single ATP synthasomes that could be readily boxed (Fig. 1B) and, based on the selection procedure described under “Experimental Procedures,” it allowed for the selection of 7506 images of the type shown in Fig. 1C.

**Verification of the Presence of PIC and ANC within ATP Synthasomes and Localization within the Basepiece**—To confirm our earlier finding that PIC and ANC co-localize with the ATP synthase (12) and establish their location within the resultant ATP synthasome, we subjected dispersed preparations to immuno-EM analysis. Here, a primary antibody to either PIC or ANC was first added, followed by the addition of a gold-labeled secondary antibody and then the negative stain. Representative photographs of many such ATP synthasomes always revealed the interaction of the antibodies with the basepiece as shown in Fig. 1, D and E. Moreover, in all cases examined, the PIC and ANC antibodies bound non-centrally in the basepiece, *i.e.* away from the center where the subunits a, c, and part of b were expected to form the proton-translocating motor within  $F_0$ .

**Assessment of the Structural Integrity of the ATP Synthasome and the Stoichiometry of its Components, *i.e.* ATP Synthase, PIC, and ANC**—Previous studies have already provided some evidence for the structural integrity of the ATP synthasome, as we have shown that the PIC/ $\beta$  and the ANC/ $\beta$  ratio remain nearly constant (1–1.3) throughout the purification from the crude membrane fraction to the final sucrose purified preparation (note that  $\beta$  refers to the catalytic subunit of the ATP synthase). To gain additional insight into the structural integrity of the ATP synthasome complex, we solubilized the final purified membrane bound form in one other detergent, *n*-decyl- $\beta$ -D-thiomaltopyranoside, which is known to preserve its ATPase activity and inhibition to oligomycin (12). The solubilized ATP synthasome was layered onto a bed of 25 ml of 25% sucrose and subjected to centrifugation at 25,000 rpm as described previously (12). Fig. 2A shows that the ATP synthasome sedimented as a single peak based both on protein and

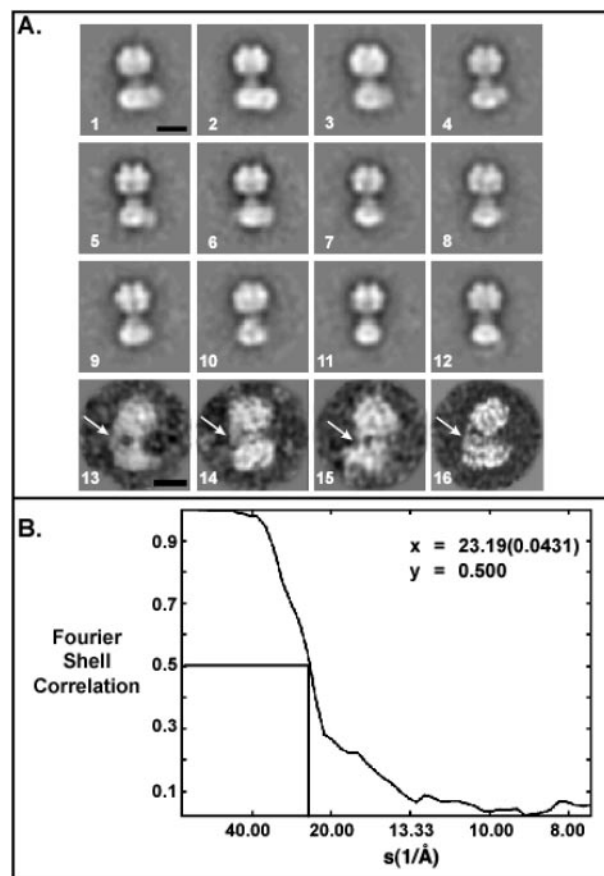


Fig. 3. A, representative, averaged, two-dimensional images of ATP synthasomes used to build the final model. The 7506 raw images were band pass-filtered, normalized, contrast transfer function phase-corrected, and iteratively aligned (25). The aligned images were then classified to produce 25 class averages. Representative class averages are shown in panels 1–12, of which 1–6 clearly show what appears to be a two-domain organization of the basepiece. A side stalk is clearly observed in some single images, *e.g.* panels 13–16 (arrows), but not at a frequency or consistent clarity to be distinctly revealed in class averages. The scale bars equal 100 Å. B, convergence plot of the final model to obtain the resolution. The self-consistency of the final model was evaluated by the Fourier shell correlation (26) of two models independently reconstructed from even- and odd-numbered raw images. The resolution is 23 Å using the 0.5 threshold criteria (see “Experimental Procedures”).

ATPase activity measurements. In no other place in the gradient was protein found, a finding that would be expected if either the much smaller PIC or ANC molecules had dissociated from the ATP synthase. Rather, as expected, their location was found to correlate with protein and activity.

The above and previous experiments (12) suggested that the ATP synthase, PIC, and ANC components that comprise the ATP synthasome are in a well defined supercomplex in which its component parts exhibit a fixed stoichiometry, the most likely of which is 1:1:1. To determine whether this is the case, we took advantage of available sequence data for each of the 17 different subunit types of the complex, the number of sulfhydryl groups in each, and known subunit stoichiometries. From this data we calculated that each ATP synthasome complex should have a total of 34–38 free sulfhydryl groups if the stoichiometric ratio of its component parts is 1:1:1. As shown in Fig. 2B, the actual determination of the number of available sulfhydryl groups by the 5,5'-dithiobis(2-nitrobenzoic acid) reagent as described under “Experimental Procedures” gives a value of  $39 \pm 3$ , which is very close to that predicted. In summary, the above studies support the view that the ATP synthasome complex is a well defined, structurally intact com-

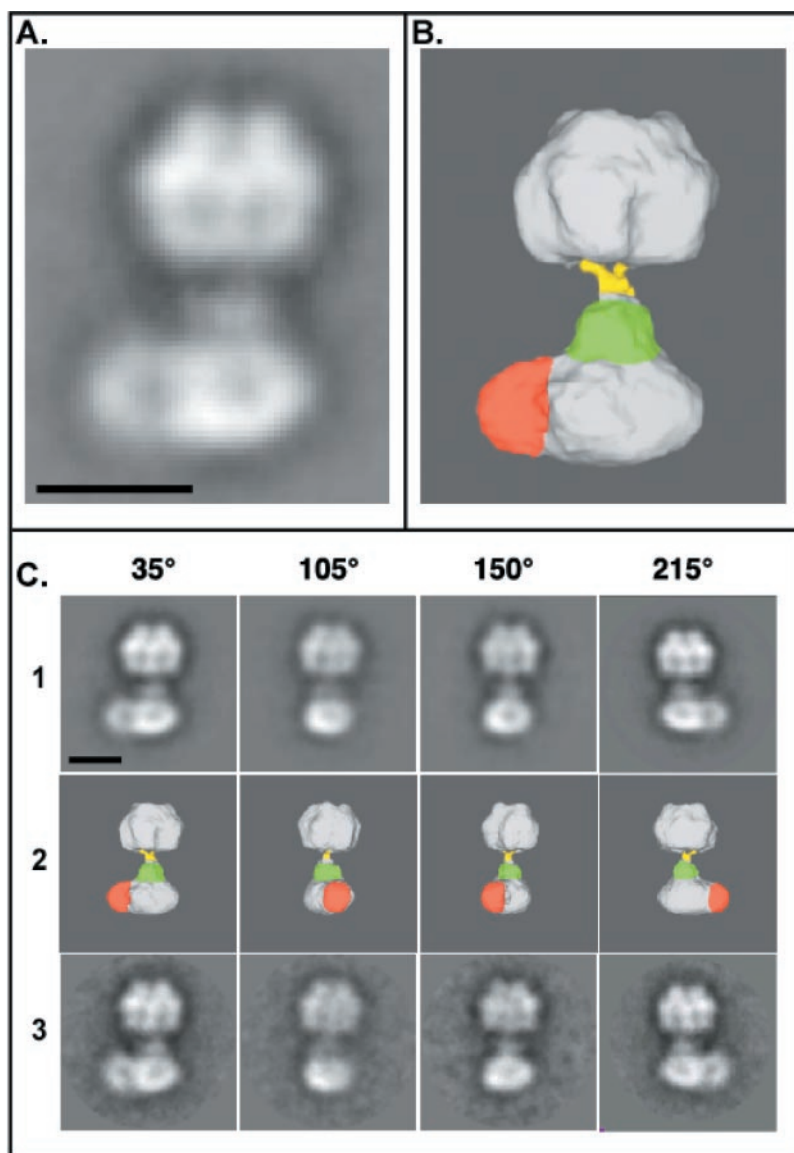


FIG. 4. *A* and *B*, projection and isosurface views at 35° of the final three-dimensional model of the reconstructed mitochondrial ATP synthasome. The most obvious structural features of the final model are an “oblong” basepiece consisting of two domains (*white* and *red*), a central mass or collar (*green*) surrounding the connecting stalk (*yellow*) just above the basepiece, and, finally, a near spherical headpiece. The scale bar equals 100 Å. *C*, a gallery of different views of the final model. Views are presented at the different angles shown at the *top*, with *row 1* depicting projection views, *row 2* depicting isosurface views contoured at 3  $\sigma$  by the program “Chimera” (36), and *row 3* depicting class averages of raw images. The scale bar equals 100 Å.

plex and that binding interactions between the ATP synthase, PIC, and ANC are likely to exist.

**Two Dimensional Analysis of ATP Synthasomes**—Fig. 3A depicts 12 of 25 class averages obtained by two-dimensional analysis of the 7506 raw ATP synthasome images as described under “Experimental Procedures.” The tripartite structure consisting of a near spherical headpiece, a basepiece, and a connecting stalk is very clear, with the headpiece showing significant substructure. Most notable, however, as concerns this report is that in some class averages (e.g. Fig. 3A, panels 1–6) the basepiece is oblong, revealing what appear to be two distinct domains. Although a side stalk projecting from the basepiece to the headpiece could be clearly observed in a number of raw images as shown in Fig. 3A, panels 13–16, class averages (not presented) only faintly revealed this structural feature. This is to be expected at the resolution obtained, both because of the side stalk’s narrow size and because, in many images, it remains completely or partially hidden, e.g. behind the headpiece or central stalk. Also, the side stalk has been reported recently from biochemical studies to assume more than one position (27).

**Three-dimensional Analysis of ATP Synthasomes to Provide a Final Model**—The analysis of the 7506 raw ATP synthasome images to give the final three-dimensional model reconstructed

from 56 class averages was carried out as described under “Experimental Procedures.” It is estimated to have a resolution of 23 Å from a plot (Fig. 3B) of the Fourier shell correlation (26) of two models independently reconstructed from even- and odd-numbered raw images. A projection view of the final model is shown in Fig. 4A, and an isosurface view of the three-dimensional model is presented in Fig. 4B. The most obvious structural features depicted in color in the isosurface view are a near spherical headpiece, a central stalk (the lower half of which is surrounded by a “collar”), and an oblong basepiece consisting of two domains. The larger of the two domains is connected to the central stalk, whereas the smaller domain appears as an extension. These various structural features of the final three-dimensional model are shown at different angles of rotation in Fig. 4C in projection views (*row 1*), three-dimensional isosurface views (*row 2*), and views representing class averages of raw images (*row 3*). In all views, the two-domain structure of the basepiece and a collar surrounding the lower half of the central stalk are clearly observed.

**Accommodation of PIC and ANC within the Two Domains of the Basepiece of the ATP Synthasome**—Prior to identifying possible locations of PIC and ANC within the basepiece of the ATP synthasome, we used “foldhunter,” a docking program included with EMAN (25, 28), to first dock into its three-

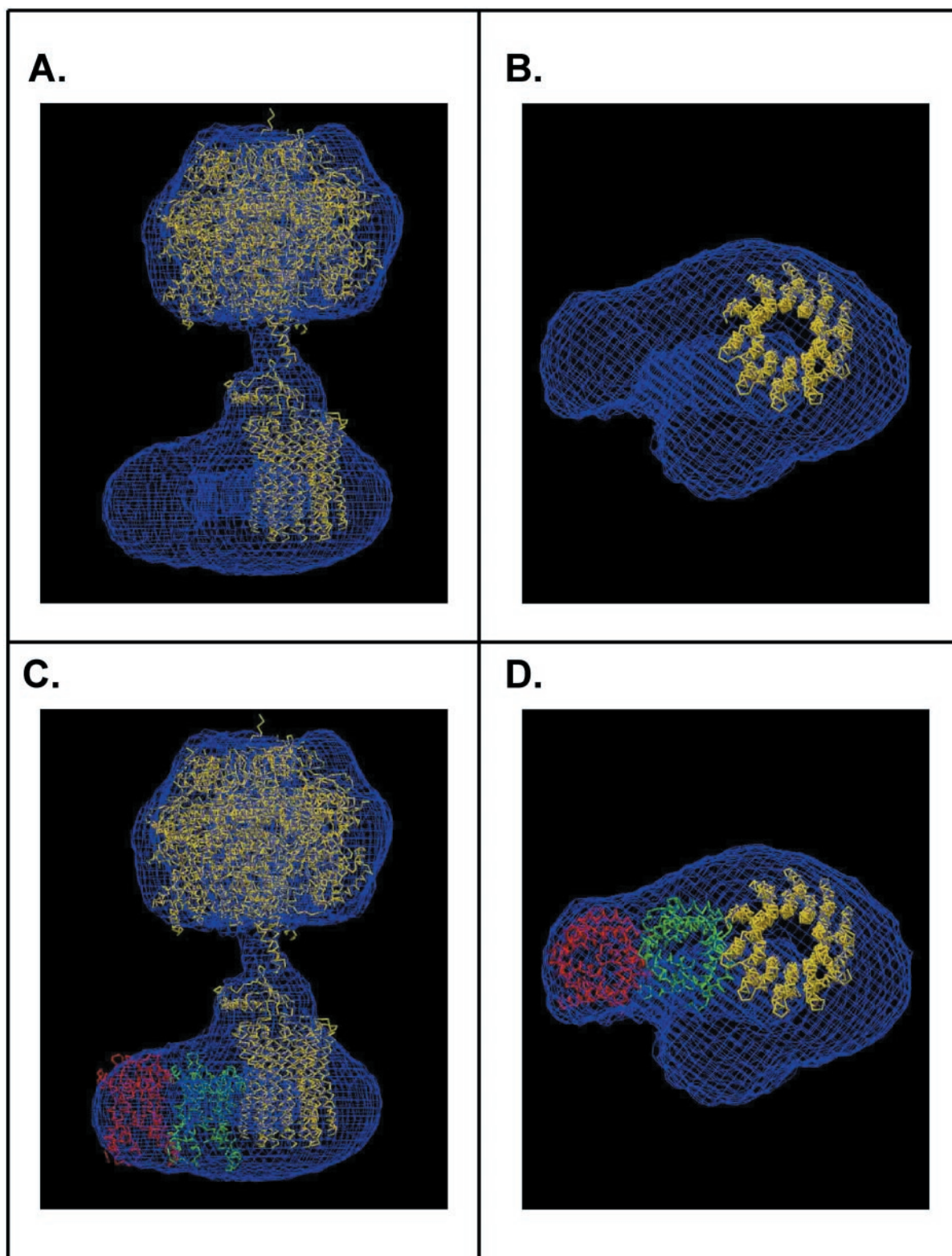


FIG. 5. *A*, a contour view of the mitochondrial ATP synthasome in which the known structure of the yeast  $F_1$ -subunit  $c_{10}$  complex (29) has been docked. The program O (30) was used to generate the contour view, and the foldhunter component of the EMAN program (25) was used for docking the  $F_1$ -subunit  $c_{10}$  complex. The *overlay* shows that the subunit  $c_{10}$  ring centrally localizes to the larger of the two basepiece domains. *B*, a top contour view of only the basepiece showing the location of the subunit  $c_{10}$  ring. Here, the position of all 10 subunits can be visualized. *C*, a contour view of the ATP synthasome in which both the known structure of the yeast  $F_1$ -subunit  $c_{10}$  complex has been docked together with the known structure of two ANC molecules. As ANC and PIC are highly homologous and have nearly identical masses, this view depicts the relative location of a predicted \*ANC/PIC heterodimer relative to the subunit  $c_{10}$  ring. Only one monomer (either PIC or ANC) can occupy the smaller of the two basepiece domains, whereas the other monomer fits in well at the end of the larger of the two domains. One monomer may interact with the subunit  $c$  ring but not overlap with it. The positions noted for PIC and ANC are consistent with the immuno-EM results presented in Fig. 1, *D* and *E*, which show, respectively, that PIC and ANC are non-centrally located in the basepiece. *D*, top contour view of a likely positional relationship of a potential PIC/ANC heterodimer to the subunit  $c$  ring. Here it will be noted that there remains sufficient mass in the front to accommodate subunit  $a$ , which is known to be adjacent to the subunit  $c_{10}$  ring, and also to accommodate part of a subunit  $b$  dimer that comprises a side stalk.

dimensional structure the 3.9-Å structure of the yeast  $F_1$ -subunit  $c_{10}$  ring complex (29). The result displayed by the program "O" (30) (Fig. 5) confirmed that the three-dimensional structure of the ATP synthasome determined in this study has the correct chirality, as both its headpiece and the  $F_1$  moiety of the yeast  $F_1$ -subunit  $c_{10}$  ring complex tilt to the same direction and at a similar angle. Moreover, if the three-dimensional structure of the ATP synthasome is mirrored to reverse the chirality, the program docks them to tilt in the opposite direction.

As expected, the subunit  $c_{10}$  ring centrally localizes within the larger of the two domains of the ATP synthasome's basepiece (Fig. 5, A and B). This finding suggested that the smaller domain of the basepiece may be the location of PIC or ANC, both of which are homologous proteins with nearly identical masses, *i.e.* 32.82 and 32.84 kDa, respectively. For this reason, the three-dimensional structure of an ANC monomer, recently determined to 2.2 Å (31), was docked in manually and shown to fit well within the smaller domain of the basepiece (Fig. 5, C and D). A second monomer, a predicted PIC equivalent, could be readily docked adjacent to it at the end of the larger basepiece domain without overlapping with the subunit  $c_{10}$  ring. These predicted locations of ANC and PIC are consistent with our immuno-EM studies showing that the two carriers localize not in the center of the basepiece but more toward its end (Fig. 1, D and E).

#### DISCUSSION

Results of studies presented here provide the first three-dimensional structural information about the mitochondrial ATP synthasome, a stoichiometric 1:1:1 ATP synthase/PIC/ANC complex that we recently isolated and characterized (12). The structure of the ATP synthasome at 23-Å resolution was achieved by image reconstruction of single ATP synthasomes dispersed in the detergent CHAPS. These studies, combined with immuno-EM studies, implicate PIC and ANC as being non-centrally located within the basepiece of the ATP synthasome, and, although they are near the more centrally located subunit  $c$  ring, do not overlap with it. Thus, these studies support an efficient and coordinated mechanism for the terminal steps of oxidative phosphorylation in mitochondria in which the players involved, *i.e.* the ATP synthase, PIC, and ANC, are located near one another in the same complex, *i.e.* the ATP synthasome (Fig. 5B).

Although a likely location of PIC and ANC is adjacent to one another, one at the end of the larger basepiece domain and the other in the smaller domain (Fig. 5, C and D), a definitive conclusion will have to await a higher resolution map, and further biochemical studies on PIC and ANC will be needed to determine whether they can each function as monomers, a heterodimer, or only in dimeric form. Recent structural studies on crystals of ANC show that the unit cell contains one monomer per asymmetric unit and that the crystal is packed as protein layers without an indication of specific dimerization within the layers (31). In contrast, however, past biochemical studies suggest that the active form of ANC is a dimer (32, 33). A dimeric form of PIC is also believed to be the active form from similar biochemical studies (34). However, each study has focused only on one transporter and not the two together, leaving open the possibility that a PIC/ANC heterodimer is really the physiological form.

Finally, as it concerns the study reported here, it would be of interest to know where the side stalk is located relative to PIC, ANC, and the subunit  $c$  ring. However, although the stalk clearly present as revealed in a number of selected raw images (Fig. 3A, panels 13–16), an insufficient number of such images were collected, for the reasons indicated above, to obtain good class averages. Therefore, the final three-dimensional model did not re-

veal this feature, and we will have to await further work.

Significantly, following the completion of work reported here, a three-dimensional structure at 32-Å resolution was determined for the ATP synthase of bovine heart by electron cryomicroscopy based on 5984 single molecules (35). This preparation, apparently lacking the transporters PIC and ANC, also shows a two-domain structure for the basepiece. Although no dimensions are reported for the heart ATP synthase structure (35), visual inspection of the images presented shows that the basepiece domain that connects to the central stalk is somewhat smaller in width than the second domain. In our ATP synthasome structure just the opposite is the case, as the basepiece domain that connects to the central stalk is much larger in width than is the second domain. This suggests that the larger of the two domains in the basepiece of the ATP synthasome may include the two domains comprising the basepiece of the heart ATP synthase. If such is the case, we should be able to observe, by using cryomicroscopy in future studies, a three-domain structure for the basepiece of the ATP synthasome.

Finally, it should be noted that, although this study has focused on the unique property of the ATP synthasome, *i.e.* the presence and location of the transporters PIC and ANC, the docking studies presented in Fig. 5B show that additional space is present throughout the three-dimensional structure. The extra space that cannot be accounted for by the "docked" structures must accommodate the remaining subunits that include the motor-related subunits  $a$  and  $b$  and the oligomycin sensitivity-conferring protein as well as the supernumerary subunits  $d$ ,  $e$ ,  $f$ ,  $g$ ,  $F_6$ , and  $A6L$ . Some of the latter subunits may contribute to the extra mass or "cap" around the top of  $F_1$ , others to a protective sheath or collar around the central stalk (Fig. 5A), and one or more to the larger basepiece domain,

*Acknowledgments*—We are grateful to Joanne Hullihen for technical assistance, to Dr. Sangjin Hong for his help in acquiring information from the data base important for estimating the total number of sulfhydryl groups in the ATP synthasome, and to David Blum.

#### REFERENCES

1. Saraste, M. (1999) *Science* **283**, 1488–1493
2. Scorrano, L., and Korsmeyer, S. J. (2003) *Biochem. Biophys. Res. Commun.* **304**, 437–444
3. Kim, J. S., He, L., and Lemasters, J. J. (2003) *Biochem. Biophys. Res. Commun.* **304**, 463–470
4. Pedersen, P. L. (1999) *J. Bioenerg. Biomembr.* **31**, 291–304
5. Kaplan, R. S. (2001) *J. Membr. Biol.* **179**, 165–183
6. Pedersen, P. L., Ko, Y. H., and Hong, S. (2000) *J. Bioenerg. Biomembr.* **32**, 23–432
7. Yoshida, M. (2001) *Nat. Rev. Mol. Cell Biol.* **2**, 669–677
8. Futai, M., Omote, H., Sambongi, Y., and Wada, Y. (2000) *Biochim. Biophys. Acta* **1458**, 276–288
9. Senior, A. E., Nadanaciva, S., and Weber, J. (2002) *Biochim. Biophys. Acta* **1553**, 188–211
10. Capaldi, R. A., and Aggeler, R. (2002) *Trends Biochem. Sci.* **27**, 154–160
11. Oster, G., and Wang, H. (1999) *Structure Fold. Des.* **7**, R67–R72
12. Ko, Y. H., Delannoy, M., Hullihen, J., Chiu, W., and Pedersen, P. L. (2003) *J. Biol. Chem.* **278**, 12305–12309
13. Catterall, W. A., Coty, W. A., and Pedersen, P. L. (1973) *J. Biol. Chem.* **248**, 7427–7431
14. Pullman, M. E., and Monroy, G. C. (1963) *J. Biol. Chem.* **238**, 3762–3769
15. Belogradov, G. I., and Hatefi, Y. (2002) *J. Biol. Chem.* **277**, 6097–6103
16. Abrahams, J. B., Leslie, A.G.W., Lutter, R., and Walker, J. E. (1994) *Nature* **370**, 621–628
17. Bianchet, M. A., Hullihen, J., Pedersen, P. L., and Amzel, L. M. (1998) *Proc. Natl. Acad. Sci. U. S. A.* **95**, 11065–11070
18. Gibbons, C., Montgomery, M. G., Leslie, A. G., and Walker, J. E. (2000) *Nat. Struct. Biol.* **7**, 1055–1061
19. Catterall, W. A., and Pedersen, P. L. (1971) *J. Biol. Chem.* **246**, 4987–4994
20. Jacobs, E. E., Jacob, M., Sanadi, D. R., and Bradley, L. B. (1956) *J. Biol. Chem.* **223**, 147–156
21. Lowry, O. H., Rosebrough, N. J., Farr, A. L., and Randall, R. J. (1951) *J. Biol. Chem.* **193**, 265–275
22. Brown, R., Jarvis, K., and Hyland, K. (1989) *Anal. Biochem.* **180**, 136–139
23. Schaffner, W., and Weissmann, C. (1973) *Anal. Biochem.* **56**, 502–514
24. Riddles, P. W., Blakely, R. L., and Zerner, B. (1983) *Methods Enzymol.* **91**, 49–60
25. Ludtke, S. J., Baldwin, P. R., and Chiu, W. (1999) *J. Struct. Biol.* **128**, 82–97

26. Frank, J. (1996) *Three Dimensional Electron Microscopy of Macromolecular Assemblies*, 1st Ed., pp. 208–209, Academic Press, San Diego, CA
27. Hardy, J. W., Grabar, T. H., Bhatt, D., and Cain, B. D. (2003) *J. Bioenerg. Biomembr.* **35**, 389–397
28. Jiang, W., Baker, M. L., Ludtke, S. J., and Chiu, W. (2001) *J. Mol. Biol.* **308**, 1033–1044
29. Stock, D., Leslie, A. G., and Walker, J. E. (1999) *Science* **286**, 1700–1705
30. Jones, T. A., Zhou, J. Y., Cowan, S. W., and Kjeldgaard, M. (1991) *Acta Crystallogr. Sect. A* **47**, 110–119
31. Pebay-Peyroula, E., Dahout-Gonzalez, C., Kahn, R., Trezeguet, V., Lauquin, G. J.-M., and Brandolin, G. (2003) *Nature* **426**, 39–44
32. Hackenberg, H., and Klingenberg, M. (1980) *Biochemistry* **19**, 548–555
33. Block, M. R., Zaccai, G., Lauquin, G. J., and Vignais, P. V. (1982) *Biochem. Biophys. Res. Commun.* **109**, 471–477
34. Schoers, A., Burkovski, A., Wohlrab, H., and Kramer, R. (1998) *J. Biol. Chem.* **273**, 14269–14276
35. Rubinstein, J. L., Walker, J. E., and Henderson, R. H. (2003) *EMBO J.* **22**, 6182–6192
36. Huang, C. C., Couch, G. S., Pettersen, E. F., and Ferrin, T. E. (1996) *Pac. Symp. Biocomput.* **1**, 724